JOURNAL OF SOLID STATE CHEMISTRY 71, 61–69 (1987)

An Investigation of the Low Oxidation State Chemistry of Rhenium in the BaO–Re–Re_2O_7 Phase Diagram

A. K. CHEETHAM AND D. M. THOMAS

University of Oxford, Chemical Crystallography Laboratory, 9 Parks Road, Oxford, OX1 3PD, England

Received August 12, 1986; in revised form January 5, 1987

The first systematic survey of the BaO–Re–Re_2O_7 phase diagram is reported, with emphasis on the reduced ternary oxides. At 800°C, the previously reported compounds $Ba_3Re_2O_9$, Ba_2ReO_5, and Ba_3ReO_6 were observed, all of which contain Re(VI) in ReO_6 octahedra. The stability of these phases is apparently due to Re–O π-bonding in and between the octahedra. The previously unknown structure of Ba_2ReO_5 was determined by powder neutron diffraction and found to be isotypic with that of $K_2VO_2F_3$ (space group *Pnma*), with $a = 7.3233(2)$, $b = 5.7745(1)$, and $c = 11.4124(2)$ Å. ReO_6 octahedra share adjacent corners to produce cis chains which are held together by 10 coordinated Ba atoms.

Introduction

The phase diagram for the Ba–Re–O system has not been reported in the literature, and although some data on compound formation within the system are available, few details are given. Here we report a systematic study carried out at 800°C under an inert atmosphere. Particular interest was paid to those ternary oxides containing rhenium in an oxidation state of less than seven.

Recently there has been growing interest in solid-state compounds containing discrete or condensed clusters of transition metal atoms. Molybdenum, which exhibits many of the chemical characteristics of rhenium, forms tetranuclear metal atom clusters in $Ba_{1.14}Mo_8O_{16}$ (*1*) and $K_2Mo_8O_{16}$ (*2*), while infinite chains of edge-sharing Mo_6 octahedra are found in $Ba_{0.62}Mo_4O_6$ (*1*) and $NaMo_4O_6$ (*3*). Low-valency rhenium is known to form metal–metal bonds in one of two basic units, Re_2O_{10} and Re_2O_8, which occur in the *Ln*–Re–O (*Ln* = lanthanide) systems (*4*); the former also occur in $BiRe_2O_6$ (*5*). However, other reduced rhenium compounds such as $Ba_3Re_2O_9$ (*6*), $Cd_2Re_2O_7$ (*7*), $PbReO_3$ (*8*), and $PbRe_2O_6$ (*9*) do not contain metal–metal bonds.

$Ba_3Re_2O_9$ is the only ternary oxide in the Ba–Re–O system to have undergone full structural characterization. It has a perovskite-related structure based on a nine-layer sequence of close-packed BaO_3 layers (*chhchhchh*). Other rhenium (VI) compounds that have been reported in this system (*10*) are Ba_2ReO_5, which Scholder claims to be isomorphic with Ba_2XO_5 (*X* = Te, Mo, W, or Os), Ba_3ReO_6, which is an ordered perovskite, and the rhombohedral phase $Ba_3ReO_6 \cdot 0.3BaO$. $BaReO_4$ is mentioned in the literature (*11*) but with little supporting evidence.

Scholder (*12*) has also investigated the

0022-4596/87 $3.00

BaO–Re_2O_7 phase diagram. Three different rhenium (VII) compounds were observed: $Ba(ReO_4)_2$, $Ba_3(ReO_5)_2$, and $Ba_5(ReO_6)_2$. The orthoperrhenate, $Ba_5(ReO_6)_2$, is thought to have a perovskite-related 24-layer structure (*13*) and the mesoperrhenate, $Ba_3(ReO_5)_2$, appears to be isostructural with the rhenium apatites, $Ba_{10}(ReO_5)_6X_2$ (X = F, Cl, Br, I, or $\frac{1}{2}CO_3$) (*14*).

Experimental

The BaO–Re–Re_2O_7 phase diagram was investigated at the compositions shown by open circles in Fig. 1. Conventional methods of solid-state synthesis were employed. The starting materials used were Re metal, ReO_2, $Ba(ReO_4)_2$, $Ba_5(ReO_6)_2$, and $BaCO_3$. The reactants were weighed out to the nearest milligram and ground together in an agate mortar, the total weight of each reaction mixture being 0.5 g. Where $BaCO_3$ was present, the reaction mixture was placed in a recrystallized alumina boat and heated to 800°C for 24 hr in an electric tube furnace under a stream of Ar gas. In all other cases, the reaction mixtures were heated for a day at 800°C in evacuated, sealed, fused-silica tubes in an electric muffle furnace.

All chemicals used were of reagent grade or better. Commercially available Re metal powder and $BaCO_3$ were used directly, and ReO_2 was prepared by thermolysis of NH_4ReO_4 under vacuum (*15*). The perrhenate was prepared by the reaction

$$Ba(OH)_2(aq) + 2NH_4ReO_4(aq) \rightarrow Ba(ReO_4)_2(s) + 2NH_3(g) + 2H_2O(l)$$

and the orthoperrhenate (*12*) by the solid-state reaction

$$Ba(ReO_4)_2(s) + 4BaCO_3(s) \xrightarrow{1200°C} Ba_5(ReO_6)_2(s) + 4CO_2(g).$$

X-ray powder patterns of the final products at various points in the phase diagram were recorded on a Philips PW 1710 diffractometer, and the barium to rhenium ratios of individual crystallites in a product mixture were obtained using a JEOL 100CX-TEMSCAN analytical electron microscope with a KEVEX Li-drifted silicon energy-dispersive X-ray detector. The "ratio method" for thin crystals described in detail by Cheetham and Skarnulis (*16*) was employed. The Ba–Lα and Re–Lβ_{1+2} X-ray emission lines of $Ba(ReO_4)_2$ were used to calculate the calibration constant, k, in the equation $x_{Ba}/x_{Re} = k(I_{Ba}/I_{Re})$, where x_{Ba}, x_{Re}, I_{Ba}, and I_{Re} represent, respectively, the concentrations and X-ray emission intensities of the two species. Analysis of 30 crystallites of $Ba(ReO_4)_2$ gave a value of 0.728(9) for k. Here and throughout this paper the number in parentheses is the estimated standard deviation (e.s.d.) in the last figure.

A neutron scattering experiment was performed on 6 g of Ba_2ReO_5 powder prepared by the reaction

$$4Ba_5(ReO_6)_2(s) + Re(s) + ReO_2(s) \rightarrow 10Ba_2ReO_5(s).$$

The reaction was carried out in a sealed silica tube by heating to 800°C for 1 day, and the diffraction profile over the range $6° \leq 2\theta \leq 144°$ was recorded over a period of 6 hr at room temperature, using the instrument D1a at ILL Grenoble operating at a wavelength of 1.909 Å with a 2θ step size of 0.05°. Electrical resistivity measurements were made on pellets of Ba_2ReO_5 (13 mm diameter × 1.5 mm thickness). A two-probe method was used and the results obtained were only qualitative in nature.

Infrared spectra of the separate reduced barium rhenium oxides suspended in CsI disks were measured on a Pye Unicam SP2000 infrared spectrometer in the region 200–4000 cm^{-1}.

Results and Discussion

This study represents the first definitive survey of the BaO–Re–Re_2O_7 system and

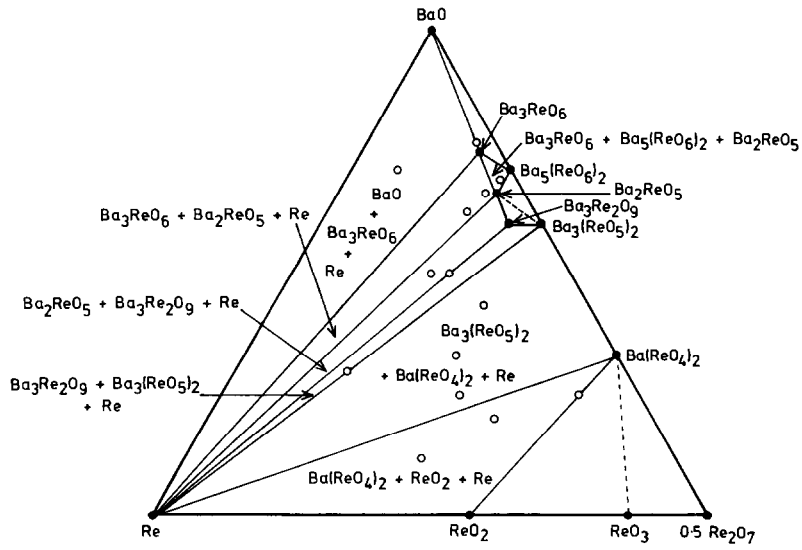

FIG. 1. The proposed BaO–Re–Re_2O_7 phase diagram at 800°C. Compositions investigated in this study are shown by open circles and solid circles represent the phases found in the system. The observed tie lines are shown by continuous lines, whereas broken lines indicate tie lines proposed after careful examination of the results.

yields results that concur with some previous reports but disagree with others. The only reduced phases in the system are $Ba_3Re_2O_9$, Ba_2ReO_5, and Ba_3ReO_6, all of which contain Re(VI); further reduction leads to the formation of Re metal. No evidence for the existence of $Ba_3ReO_6 \cdot 0.3BaO$ (*10*) or $BaReO_4$ (*11*) was found.

The results of the synthetic work at 800°C are summarized in Fig. 1, and specific reactions and their products are given in Table I. Prolonged heating gave the same products, although reaction with the silica tube to give barium silicate occurred when the temperature was raised to 1000°C. Further verification that equilibrium had been reached was given by the fact that identical results were obtained when different reactants were used to attain the same starting composition.

The preparation and crystal structure of $Ba_3Re_2O_9$ have already been reported in the literature (*6*), so no further comment is necessary. Under atmospheric conditions, this phase was completely oxidized to $Ba_3(ReO_5)_2$ within a period of 4 months.

Ba_2ReO_5 containing traces of Re metal could be synthesized as a dark gray powder. The composition was confirmed by analytical electron microscopy: analysis of 23 crystallites gave a Ba/Re ratio of 2.01(5). As previously reported (*17*), the oxygen content has been studied using an analytical electron microscope equipped with an ultrathin window X-ray detector. In agreement with Scholder and Pfeiffer (*10*), the X-ray powder pattern of this compound shows it to be isotypic with Ba_2XO_5, where X = Te, Mo, W, or Os. The structure of these phases is unknown, but careful examination of the cell parameters and X-ray intensities indicates that they are isostructural with $K_2VO_2F_3$ (*18*), which is known to contain nonlinear chains of $VO_2F_2F_{2/2}$ octahedra linked by cis-bridging fluorine atoms. The infrared spectrum of Ba_2ReO_5 (Fig. 2) shows strong absorption bands at 360 and 630 cm^{-1}, as expected for the bending and

TABLE I

RESULTS OF THE INVESTIGATION OF THE BaO–Re–Re_2O_7 PHASE DIAGRAM AT 800°C

Reaction mixture	Conditions: Temperature (°C)	Conditions: Time	Products
$5BaCO_3 + ReO_2 + Re$	800	1 day	$BaCO_3 + Ba_3ReO_6$ + trace Re + trace $Ba_3(ReO_5)_2$[a]
$9BaCO_3 + Ba(ReO_4)_2 + ReO_2$	1000	Overnight	Ba_3ReO_6 + trace $BaCO_3$ + trace $Ba_3(ReO_5)_2$[a]
$8BaCO_3 + Ba(ReO_4)_2 + ReO_2$	1000	Overnight	Ba_3ReO_6 + trace $Ba_3(ReO_5)_2$[a]
$8BaCO_3 + Ba(ReO_4)_2 + ReO_2$	500	Overnight	$BaCO_3 + Ba_3(ReO_5)_2$
$5Ba_5(ReO_6)_2 + Re$	800	3 days	$Ba_2ReO_5 + Ba_5(ReO_6)_2$ + trace Ba_3ReO_6
$2Ba_5(ReO_6)_2 + Re$	800	3 days	Ba_2ReO_5
$Ba_5(ReO_6)_2 + Re$	800	3 days	Ba_2ReO_5
$4Ba_5(ReO_6)_2 + ReO_2 + Re$	800	1 day	Ba_2ReO_5
$4Ba_2ReO_5 + ReO_2 + 3Re$	800	1 day	$Ba_3Re_2O_9$ + Re + trace Ba_2ReO_5 + trace $Ba_3(ReO_5)_2$[a]
$Ba_5(ReO_6)_2 + Ba(ReO_4)_2 +$ 10Re	800	1 day	$Ba_3(ReO_5)_2 + Ba_3Re_2O_9 +$ Re
$Ba_5(ReO_6)_2 + 2Ba(ReO_4)_2$ + 3Re	800	1 day	$Ba_3(ReO_5)_2 + Ba(ReO_4)_2 +$ trace Re
$Ba(ReO_4)_2 + ReO_2 + Re$	800	1 day	$Ba(ReO_4)_2 + ReO_2 + Re$
$0.8BaCO_3 + 5ReO_2 + Re$	800	4 days	$Ba(ReO_4)_2 + ReO_2 + Re$
$Ba(ReO_4)_2 + ReO_2$	800	4 days	$Ba(ReO_4)_2 + ReO_2$
$BaO + ReO_2$[b]	500	1 day	$Ba_3Re_2O_9 + Re$
$BaO + 2ReO_2$[b]	600	1 day	$Ba_3(ReO_5)_2 + Ba(ReO_4)_2 +$ Re
$BaO + 3ReO_2$[b]	600	1 day	$Ba(ReO_4)_2 + Re +$ Ba silicate

[a] $Ba_3(ReO_5)_2$ is an oxidation product of both Ba_3ReO_6 and $Ba_3Re_2O_9$ under atmospheric conditions.

[b] Experiments using BaO were discontinued due to difficulties in handling and reactivity with the walls of the silica reaction vessel.

stretching of ReO_6 octahedra (*19*). Thus the X-ray powder data for Ba_2ReO_5 (Table II) were indexed in the space group *Pnma* (as for $K_2VO_2F_3$) and the cell parameters refined by the least-squares method give values of $a = 7.320(2)$, $b = 5.775(1)$, and $c = 11.412(3)$ Å.

Ba_3ReO_6 was the only other low-valency ternary oxide observed in this study. Electron microscope data from 18 crystallites in the dark gray product gave the Ba/Re ratio as 3.00(9), but attempts to confirm the oxygen content in this barium-rich phase failed due to fluorescence of the oxygen–K X-ray emission line by the Ba–*M* line (*17*). The X-ray powder pattern (Table III) cannot be satisfactorily indexed on the basis of the tetragonal cell proposed by Sleight *et al.* (*20*) as the lines observed at $d_{obs} = 3.327$ and 2.209 Å remain unaccounted for, and

TABLE II

THE X-RAY POWDER PATTERN OF Ba_2ReO_5

hkl	d_{obs} (Å)	d_{calc} (Å)	$(100I/I_o)_{obs}$	$(100I/I_o)_{calc}$
101	6.116	6.124	11	11
002	5.662	5.674	11	11
102	4.476	4.480	4	4
111	4.200	4.196	9	9
112	3.541	3.537	4	3
201	3.475	3.473	20	18
103	3.365	3.364	3	2
013	3.168	3.167	100	100
210, 202	3.078	3.082, 3.072	41	29, 32
211	2.977	2.975	36	36
020	2.880	2.879	47	49
212	2.711	2.711	28	33
203	2.631	2.631	16	17
114	2.409	2.409	8	8
204	2.245	2.245	6	7
221	2.219	2.219	14	16
123	2.189	2.190	5	5
105	2.174	2.174	5	7
015	2.118	2.118	8	6
222	2.102	2.103	24	27
303	2.050	2.050	4	4
223	1.944	1.944	18	19
205	1.934	1.933	9	8
006	1.898	1.899	6	7
215	1.833	1.833	10	9
224	1.771	1.772	2	2
410	1.741	1.742	13	13
033	1.715	1.715	12	15
230	1.701	1.701	4	5
231	1.683	1.682	6	6
412	1.667	1.666	4	2
403	1.646	1.647	10	10
232	1.630	1.630	6	7
216	1.617	1.618	8	8
225	1.607	1.606	7	7
026	1.586	1.586	7	8
134	1.557	1.557	2	2
126	1.550	1.550	3	2

least-squares refinement of the cell parameters yields e.s.d.'s that are unacceptably large when compared with those obtained for Ba_2ReO_5; the final values of the cell parameters are $a = 8.65(1)$ and $c = 8.34(2)$ Å. However, by comparison with the powder

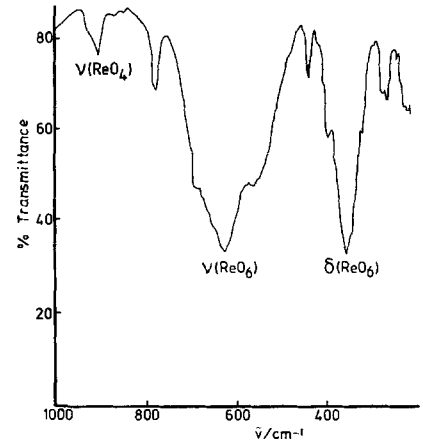

FIG. 2. The infrared spectrum of Ba_2ReO_5. The $\nu(ReO_4)$ peak shows the presence of $Ba(ReO_4)_2$ arising from partial hydrolysis of the product in the CsI disk.

pattern of Ba_3WO_6 (*21*), it seems likely that the structure is a distorted form of the cryolite structure, and the two strong bands at 390 and 600 cm^{-1} in the infrared spectrum

TABLE III

THE X-RAY POWDER PATTERN OF Ba_3ReO_6

hkl[a]	d_{obs} (Å)	d_{calc} (Å)	$(100I/I_o)_{obs}$
111	4.940	4.935	17
200	4.328	4.327	6
121	3.511	3.511	6
Unindexed	3.327	—	15
220	3.050	3.059	100
202	3.005	3.003	93
131	2.599	2.599	9
113	2.529	2.531	6
302	2.379	2.372	5
Unindexed	2.209	—	14
400	2.159	2.162	19
004	2.082	2.085	9
242	1.758	1.754	20
224	1.722	1.722	10
151	1.660	1.660	11

[a] Lines indexed according to Sleight's tetragonal cell: $a = 8.65$, $c = 8.33$ Å.

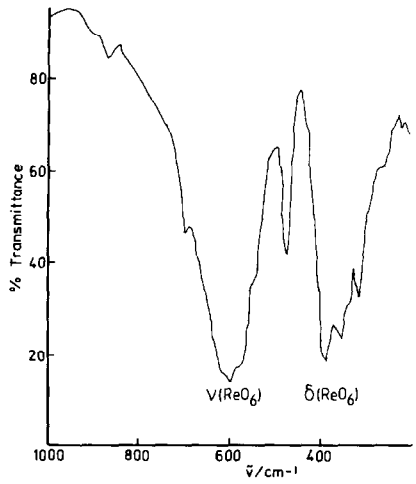

FIG. 3. The infrared spectrum of Ba_3ReO_6.

(Fig. 3) indicate the octahedral coordination of rhenium expected in this case. It is possible that more than one phase of Ba_3ReO_6 is present as suggested by Scholder and Pfeiffer (*10*).

$Ba_3Re_2O_9$, Ba_2ReO_5, and Ba_3ReO_6 all contain the octahedral ReO_6 moiety, and the stability of Re(VI) in these compounds, in contrast with the oxidation states of IV to V found in the reduced rare earth and posttransition metal rhenium oxides, is attributed to the presence of Re–O π-bonding in and between these units. Pi-bonding due to the mixing of transition metal t_{2g} and oxygen $p\pi$ orbitals has been established in ReO_3 and transition metal oxides with the perovskite structure (*22*). Kamata and Nakamura (*23*) have shown that for perovskite compounds ABO_3, the covalency of the *B*–O–*B* bonding is closely related to the Coulomb potentials due to the *A* and *B* cations. The charge/radius ratio of the *A* cation is a measure of the disturbance of the covalent *B*–O bonding by *A*. A related argument applied to the rare earth and bismuth rhenium oxides, where the acidity of the *A* cation is greater than that on Ba^{2+}, may explain why the reduced compounds in these systems are stabilized by Re–Re bonding rather than by Re–O π-overlap (*4*, *5*).

In the three reduced barium rhenium oxides, a low O/Re ratio gives rise to a structure of high connectivity: in $Ba_3Re_2O_9$ each ReO_6 octahedron shares three oxygen atoms with three other octahedra, whereas chains of cis-linked octahedra are present in Ba_2ReO_5 and Ba_3ReO_6 contains isolated ReO_6 units. Unlike the perovskite-related structures of $Ba_3Re_2O_9$ and Ba_3ReO_6, Ba_2ReO_5 does not have a close-packed structure (*24*).

The powder neutron diffraction data obtained from Ba_2ReO_5 in the range $28° < 2\theta < 123.5°$ were analyzed using a version of the Rietveld profile analysis program (*25*). The data were contaminated by trace amounts of Re metal in the sample, and the affected region of the profile was excluded from the structure refinements, as were the low-angle, asymmetric peaks. The structure was refined from a starting model with the atomic coordinates of $K_2VO_2F_3$ (*18*); the scattering lengths used were those supplied by Bacon (*26*). Least-squares refinement of 13 positional parameters, 3 isotropic temperature factors, and the usual profile parameters gave a weighted profile *R*-value of 9.82%. Details are given in Table IV and the observed, calculated, and difference profiles are plotted in Fig. 4. The cell parameters (space group *Pnma*) refined to give the following values: $a = 7.3233(2)$, $b = 5.7745(1)$, $c = 11.4124(2)$ Å. The final atomic coordinates and temperature factors are listed in Table IV, and the bond lengths and bond angles are given in Table V.

The structure of Ba_2ReO_5 is shown in Figs. 5 and 6. ReO_6 octahedra share two adjacent vertices to form infinite cis-bridged chains running parallel to the *b*-axis between 10 coordinate Ba atoms. This is isostructural with Rb_2CrF_5 (*27*), Rb_2FeF_5 (*28*), Cs_2DyCl_5 (*24*), and of course $K_2VO_2F_3$; K_2VOF_4 (*29*) and $(NH_4)_2VOF_4$ (*30*) crystallize in the noncentrosymmetric form

TABLE IV

DETAILS OF THE REFINEMENT AND FINAL ATOMIC POSITIONS AND ISOTROPIC TEMPERATURE FACTORS FOR Ba_2ReO_5

Space group: *Pnma*
a = 7.3233(2), b = 5.7745(1), c = 11.4124(2) Å
Gaussian half-width parameters: U = 2023(94), V = −4045(174), W = 3594(76)
No. of reflections: 227
No. of data points: 1822
No. of parameters: 24
R_{pr} = 9.18%; R_{wpr} = 9.82%
R_{exp} = 9.66%; χ^2 = 1.03

Atom	*x/a*	*y/b*	*z/c*	*B* (Å²)[a]
Ba(1)	0.0252(5)	0.25	0.2136(3)	0.89(5)
Ba(2)	0.3319(6)	0.25	0.9213(3)	0.89(5)
Re	0.3261(3)	0.25	0.5664(2)	0.47(4)
O(1)	0.3272(3)	−0.0123(4)	0.1189(2)	0.94(3)
O(2)	0	0	0	0.94(3)
O(3)	0.2218(4)	0.25	0.4136(3)	0.94(3)
O(4)	0.4771(5)	0.25	0.6920(3)	0.94(3)

[a] The temperature factors of barium and oxygen atoms, respectively, were constrained to be equal.

TABLE V

BOND LENGTHS (Å) AND BOND ANGLES (°) FOR Ba_2ReO_5

		2× Re–O(1)	1.872(3)
		2× Re–O(2)	2.069(2)
		Re–O(3)	1.810(4)
		Re–O(4)	1.904(4)
2× Ba(1)–O(1)	2.837(4)	2× Ba(2)–O(1)	2.717(4)
2× Ba(1)–O(1)	2.890(4)	2× Ba(2)–O(1)	2.886(4)
2× Ba(1)–O(2)	2.839(4)	2× Ba(2)–O(2)	2.966(4)
Ba(1)–O(3)	2.654(6)	2× Ba(2)–O(3)	2.915(6)
Ba(1)–O(3)	2.698(6)	Ba(2)–O(4)	2.825(5)
2× Ba(1)–O(4)	2.898(5)	Ba(2)–O(4)	2.902(5)

O(1)–Re–O(1)	94.3
O(1)–Re–O(2)	88.6 (*cis*), 176.5 (*trans*)
O(1)–Re–O(3)	96.5
O(1)–Re–O(4)	93.0
O(2)–Re–O(2)	88.5
O(2)–Re–O(3)	85.1
O(2)–Re–O(4)	84.9
O(3)–Re–O(4)	166.0
Re–O(2)–Re	180.0

Note. Estimated standard deviation in bond angles is 1°.

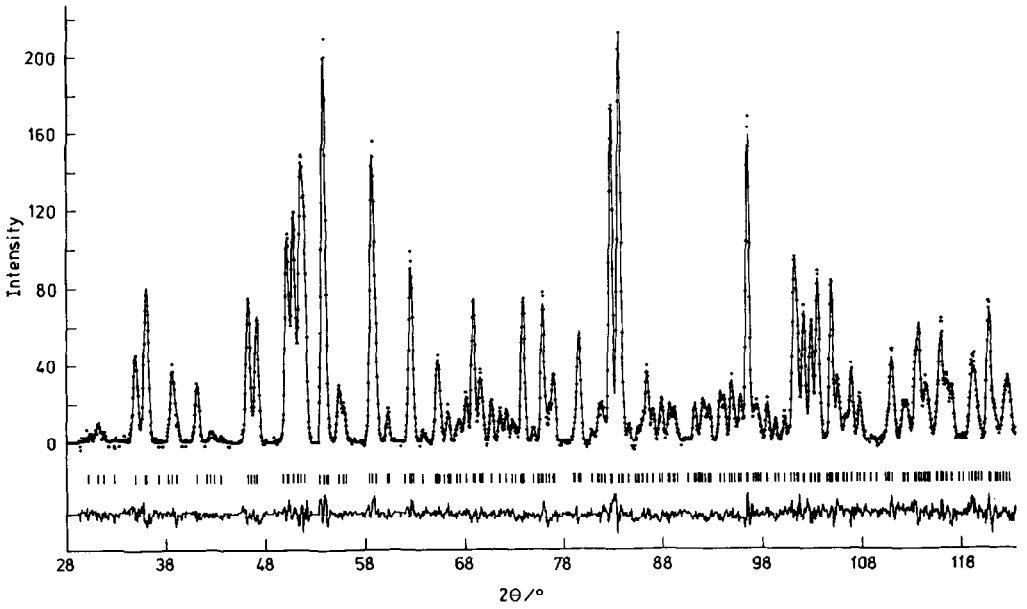

FIG. 4. The observed (dots), calculated (continuous line), and difference profiles for Ba_2ReO_5. Reflection positions are shown as bars. λ = 1.909 Å.

of this structure. Although this is one of the four main structure types presently known for A_2MF_5 fluorides, this is the first time the structure has been confirmed for a ternary oxide. Both cis and trans configurations of the MF_5 chain are known in A_2MF_5 fluorides. The K_2FeF_5-type structure (*31*) has cis chains similar to those in Ba_2ReO_5, but the repeat unit of the chain contains eight, instead of two, octahedra; in comparison, trans chains are present in Tl_2AlF_5 (*32*) and $(NH_4)_2MnF_5$ (*33*).

In Ba_2ReO_5, the Re–O(2)–Re angle is 180°, as is the case for all centrosymmetric structures of the $K_2VO_2F_3$ type. By contrast, the bridging Fe–F–Fe angles in the cis chains of K_2FeF_5 range from 162.0 to 173.4°, with an average value of 170.4°. The angle of 180° in Ba_2ReO_5 is taken to indicate π-bonding between adjacent Re atoms via

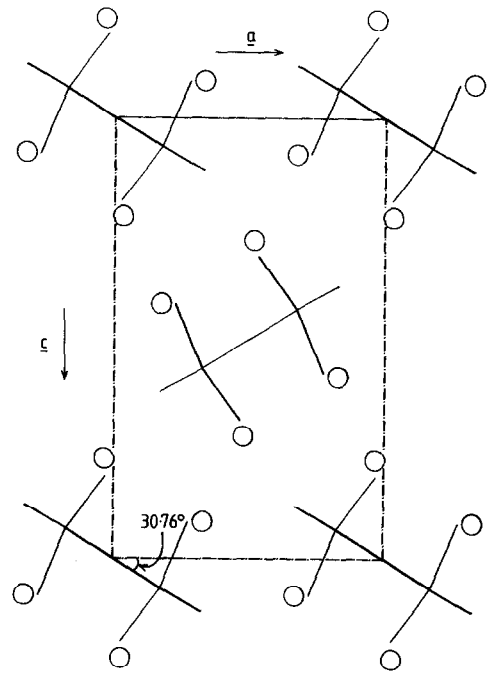

FIG. 6. Schematic structure of Ba_2ReO_5 looking along the direction of the cis-bridged chains. Barium positions are shown as open circles.

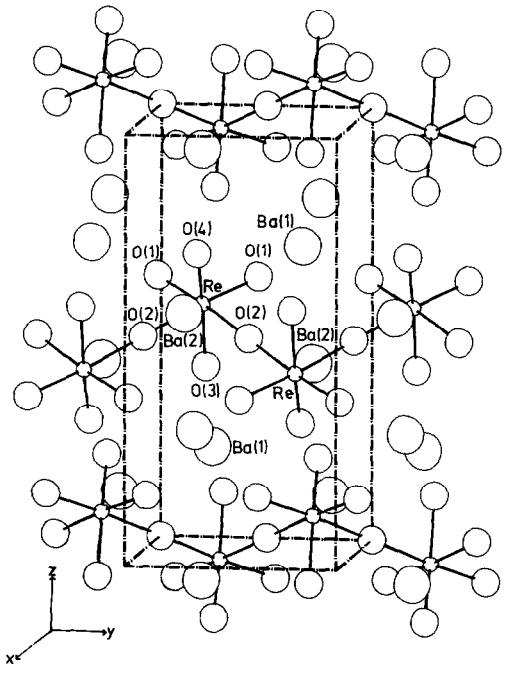

FIG. 5. The structure of Ba_2ReO_5, showing the cis chains of corner-sharing ReO_6 octahedra running parallel to *b*.

the bridging oxygen, as in the linear $[Cl_5Re–O–ReCl_5]^{4-}$ anion (*34*). Like $Ba_3Re_2O_9$ (*6*), Ba_2ReO_5 has a high room-temperature resistivity ($\rho \sim 10^7\ \Omega$ cm), which is no doubt a consequence of the orthogonality of the Re t_{2g} orbitals required to take part in π-bonding to cis oxygen atoms.

As expected from the structures of Rb_2CrF_5 and Cs_2DyCl_5, the Re–O (bridging) bond length (2.069(2) Å) is the longest Re–O distance in the ReO_6 octahedron. The Re–O(3) and Re–O(4) bonds bend toward the longer Re–O(2) bridging bonds so that the angle O(3)–Re–O(4) is 166.0°; cf. 174.43° in Rb_2CrF_5, 166.4° in $CsDyCl_5$, and 156.3° in the more distorted oxyfluoride $K_2VO_2F_3$. The Re–O(3) bond length (1.810(4) Å) is significantly shorter than the other Re–O (terminal) bonds, and this may be indicative of an antiferroelectric displace-

ment in the ReO_6 octahedron, as seen in NbO_2 (*35*). Overall the average Re–O bond length in Ba_2ReO_5 is 1.933 Å, which is comparable to previously determined values in other Re(VI) compounds: 1.875 Å in ReO_3 (*36*), 1.961 Å in $Ba_3Re_2O_9$ (*6*), and 1.923 Å in Ca_3ReO_6 (*37*).

Acknowledgments

We are grateful to the SERC for a studentship (D.M.T.) and the provision of neutron diffraction facilities at ILL, Grenoble. We also thank J. P. Attfield for collecting the neutron data.

References

1. C. C. Torardi and R. E. McCarley, *J. Solid State Chem.* **37,** 398 (1981).
2. C. C. Torardi and J. C. Calabrese, *Inorg. Chem.* **23,** 3281 (1984).
3. C. C. Torardi and R. E. McCarley, *J. Amer. Chem. Soc.* **101,** 3963 (1979).
4. G. Baud, J.-P. Besse, M. Capestan, and R. Chevalier, *Ann. Chim. (Paris)* **7,** 615 (1982).
5. A. K. Cheetham and A. R. Rae Smith, *Mater. Res. Bull.* **16,** 7 (1981).
6. B. L. Chamberland and F. C. Hubbard, *J. Solid State Chem.* **26,** 79 (1978); C. Calvo, H. N. Ng, and B. L. Chamberland, *Inorg. Chem.* **17,** 699 (1978).
7. P. C. Donohue, J. M. Longo, R. D. Rosenstein, and L. Katz, *Inorg. Chem.* **4,** 1152 (1965).
8. J. M. Longo, P. M. Raccah, and J. B. Goodenough, *Mater. Res. Bull.* **4,** 191 (1969).
9. I. Wentzell, H. Fuess, J. W. Bats, and A. K. Cheetham, *Z. Anorg. Allg. Chem.* **528,** 48 (1985).
10. R. Scholder and P. P. Pfeiffer, *Angew. Chem. Int. Ed. Engl.* **2,** 265 (1963).
11. E. A. Boudreaux and L. N. Mulay, *in* "Theory and Applications of Molecular Paramagnetism," p. 154, Wiley, London (1976).
12. R. Scholder and K. L. Huppert, *Z. Anorg. Allg. Chem.* **334,** 209 (1964).
13. J. M. Longo, L. Katz, and R. Ward, *Inorg. Chem.* **4,** 235 (1965).
14. E. J. Baran, G. Baud, and J.-P. Besse, *Spectrochim. Acta, Part A* **39,** 383 (1983).
15. W. Freundlich and A. Deschanvres, *C.R. Acad. Sci. Paris* **245,** 1809 (1957).
16. A. K. Cheetham and A. J. Skarnulis, *Anal. Chem.* **53,** 1060 (1981).
17. A. K. Cheetham, A. J. Skarnulis, D. M. Thomas, and K. Ibe, *J. Chem. Soc., Chem. Commun.*, 1603 (1984).
18. R. R. Ryan, S. H. Mastin, and M. J. Reisfeld, *Acta Crystallogr., Sect. B* **27,** 1270 (1971).
19. E. J. Baran, *Monatsh. Chem.* **107,** 1327 (1976).
20. A. W. Sleight, J. Longo, and R. Ward, *Inorg. Chem.* **1,** 245 (1962).
21. E G. Steward and H. P. Rooksby, *Acta Crystallogr.* **4,** 503 (1951).
22. A. Ferretti, D. B. Rogers, and J. B. Goodenough, *J. Phys. Chem. Solids* **26,** 2007 (1965).
23. K. Kamata and T. Nakamura, *J. Phys. Soc. Japan* **35,** 1558 (1973).
24. G. Meyer, *Z. Anorg. Allg. Chem.* **469,** 149 (1980).
25. H. M. Rietveld, *J. Appl. Crystallogr.* **2,** 65 (1969).
26. G. E. Bacon, "Neutron Diffraction," 3rd ed., Oxford Univ. Press, Oxford (1975).
27. C. Jacoboni, R. de Pape, M. Poulain, J. Y. Le Marouille, and D. Grandjean, *Acta Crystallogr., Sect. B* **30,** 2688 (1974).
28. A. Tressaud, J. L. Soubeyroux, J. M. Dance, R. Sabatier, P. Hagenmuller, and B. M. Wanklyn, *Solid State Commun.* **37,** 479 (1981).
29. K. Waltersson and B. Karlsson, *Cryst. Struct. Commun.* **7,** 459 (1978).
30. P. Bukovec and L. Golic, *Acta Crystallogr., Sect. B* **36,** 1925 (1980).
31. M. Vlasse, G. Matejka, A. Tressaud, and B. M. Wanklyn, *Acta Crystallogr., Sect. B* **33,** 3377 (1977).
32. C. Brosset, *Z. Anorg. Allg. Chem.* **235,** 139 (1937).
33. D. R. Sears and J. L. Hoard, *J. Chem. Phys.* **50,** 1066 (1969).
34. J. C. Morrow, *Acta Crystallogr.* **15,** 851 (1962).
35. A. K. Cheetham and C. N. R. Rao, *Acta Crystallogr., Sect. B* **32,** 1579 (1976).
36. A. Magnéli, *Acta Chem. Scand.* **11,** 28 (1957).
37. A. K. Cheetham and D. M. Thomas, unpublished results.